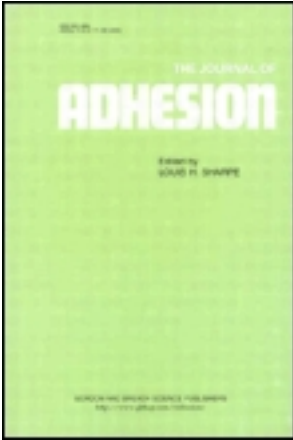


This article was downloaded by: [Indian Institute of Technology Kanpur]

On: 16 December 2011, At: 10:56

Publisher: Taylor & Francis

Informa Ltd Registered in England and Wales Registered Number: 1072954 Registered office: Mortimer House, 37-41 Mortimer Street, London W1T 3JH, UK



## The Journal of Adhesion

Publication details, including instructions for authors and subscription information:

<http://www.tandfonline.com/loi/gadh20>

### Contact of a Rigid Cylindrical Punch with an Adhesive Elastic Layer

Ravi Dalmeya<sup>a</sup>, Ishan Sharma<sup>a</sup>, Chandrashekhar Upadhyay<sup>b</sup> & Akash Anand<sup>c</sup>

<sup>a</sup> Mechanics Group, Department of Mechanical Engineering, Indian Institute of Technology Kanpur, Kanpur, Uttar Pradesh, India

<sup>b</sup> Department of Aerospace Engineering, Indian Institute of Technology Kanpur, Kanpur, Uttar Pradesh, India

<sup>c</sup> Department of Mathematics and Statistics, Indian Institute of Technology Kanpur, Kanpur, Uttar Pradesh, India

Available online: 16 Dec 2011

To cite this article: Ravi Dalmeya, Ishan Sharma, Chandrashekhar Upadhyay & Akash Anand (2012): Contact of a Rigid Cylindrical Punch with an Adhesive Elastic Layer, The Journal of Adhesion, 88:1, 1-31

To link to this article: <http://dx.doi.org/10.1080/00218464.2011.610224>

PLEASE SCROLL DOWN FOR ARTICLE

Full terms and conditions of use: <http://www.tandfonline.com/page/terms-and-conditions>

This article may be used for research, teaching, and private study purposes. Any substantial or systematic reproduction, redistribution, reselling, loan, sub-licensing, systematic supply, or distribution in any form to anyone is expressly forbidden.

The publisher does not give any warranty express or implied or make any representation that the contents will be complete or accurate or up to date. The accuracy of any instructions, formulae, and drug doses should be independently verified with primary sources. The publisher shall not be liable for any loss, actions, claims, proceedings, demand, or costs or damages whatsoever or howsoever caused arising directly or indirectly in connection with or arising out of the use of this material.

## Contact of a Rigid Cylindrical Punch with an Adhesive Elastic Layer

RAVI DALMEYA<sup>1</sup>, ISHAN SHARMA<sup>1</sup>, CHANDRASHEKHAR  
UPADHYAY<sup>2</sup>, and AKASH ANAND<sup>3</sup>

<sup>1</sup>*Mechanics Group, Department of Mechanical Engineering, Indian Institute of  
Technology Kanpur, Kanpur, Uttar Pradesh, India*

<sup>2</sup>*Department of Aerospace Engineering, Indian Institute of Technology Kanpur,  
Kanpur, Uttar Pradesh, India*

<sup>3</sup>*Department of Mathematics and Statistics, Indian Institute of Technology Kanpur,  
Kanpur, Uttar Pradesh, India*

*We investigate the contact of a cylindrical punch with an adhesive elastic layer or film bonded to a rigid substrate. The classical assumption of Hertzian contact are coupled with tools of fracture mechanics to resolve the contact problem. The contact edge's singularity is resolved by introducing a Dugdale-Barenblatt model for the adhesive zone extending in front of the contact region. Exact governing equations so obtained are solved by a semi-analytical technique employing Chebyshev polynomials. We also extend the useful JKR approximation to the indentation of elastic layers as a particular case of our general solution.*

**KEYWORDS** *Adhesion; Contact mechanics; Dugdale model; Elastic layers; Hertz contact; JKR approximation*

### 1. INTRODUCTION

With increased emphasis on manufacturing adhesives, providing protective coating, etc., the interest in thin films continues to grow. The mechanical properties of such elastic layers are not as easy to obtain as those of bulk materials, as the analysis of the various indentation tests is complicated.

---

Received 15 January 2011; in final form 13 April 2011.

One of a Collection of papers honoring Chung-Yuen Hui, the recipient in February 2011 of *The Adhesion Society Award for Excellence in Adhesion Science, Sponsored by 3M*.

Address correspondence to Ishan Sharma, Department of Mechanical Engineering, Indian Institute of Technology Kanpur, Kanpur, Uttar Pradesh 208016, India. E-mail: ishans@iitk.ac.in

Semi-analytical techniques have been developed to investigate the indentation of a cylindrical punch on an elastic layer by several authors, e.g., [1–4]), etc.; see [5, Sec. 6.5] for a more complete survey. More recently, the axi-symmetric indentation of coated elastic materials was considered with the help of Chebyshev polynomials by [6], and by [7] *via* a self-consistent numerical scheme. Similarly, it became necessary to analyze indentation tests of *adhesive* elastic layers. Several authors have provided an extension of the popular JKR approximation of [8] to adhesive layers, and these include [9] who employed finite element calculations to appropriately modify the JKR theory, [10] who carried out an energy analysis in the spirit of the original paper of [8] while employing an approximate axi-symmetric contact pressure distribution obtained for *incompressible* films in [11]. At the same time [12], employed their self-consistent numerical scheme to extend to elastic layers the fracture mechanics approach utilized by [13] to unify the analysis of adhesive contact of same-sized spheres. This latter problem has also been analyzed by [14]. Here, we present a semi-analytical scheme that allows for a simple, transparent, and more straightforward computation of the adhesive contact of a rigid punch to an adhesive elastic layer resting on a substrate. For brevity, we will restrict ourselves to the case when the layer is bonded to a rigid substrate; neither of these are restrictive assumptions. Furthermore, while we consider a *two-dimensional* scenario, extension to an axi-symmetric case is immediate.

In indentation problems, a primary aim is to relate the total applied indenting force to the contact area and the indenter's displacement in terms of the system's mechanical properties. To achieve this, the surface displacements are related to the surface tractions via an integral equation; *cf.* Section 3.1. It is hoped that the solution of this integral equation, along with the requirement that the contact pressure add up to the applied far-field force, will provide us with a unique solution to the contact pressure distribution, from which other relevant parameters may be obtained. However, the solution to the aforementioned integral equation includes a pressure distribution that, while integrable over the contact area, becomes unbounded at the contact's boundary. Thus, in addition to balancing the total applied force, a closure condition is required to address this singularity. For example, as discussed in Section 4.2 of [15], the general solution for the contact pressure in the Hertz problem has finite and infinite parts regulated by unknown constants  $p_0$  and  $p'_0$ . A unique solution for *smooth* and *non-adhesive* spheres is only obtained when the contact pressure is presumed to vanish at the contact zone's edges, as in this case we expect the boundary stresses to be continuous across the contact zone. Similarly, for *adhesive* and *soft* elastic spheres [8], retain the singular part of the contact pressure field, but prescribe the extra condition that the system's total potential energy, composed of elastic and surface energies, is minimized; this is now termed the *JKR approximation*. Analogously, assuming that the contact zone remains unchanged for *hard* adhesive spheres, [16] were able to obtain a unique answer for the contact

pressure distribution; this became the *DMT approximation*. A detailed discussion of the latter two approximate approaches was provided by [13], who also managed to unite these two apparently divergent viewpoints.

Maugis [13] considered the indentation of an adhesive elastic half-space by a rigid punch, noting that this is equivalent to the contact of two same-sized adhesive elastic spheres. To this end [13], appealed to the physical analogy between contact problems and crack closure/opening analyses in fracture mechanics. In fracture mechanics, a *cohesive zone* is often introduced to relieve the unphysical infinite stress concentration predicted at crack tips by linear elastic fracture mechanics; see *e.g.*, [17, p. 486]. This stress concentration is regulated by an unknown *stress intensity factor*. Within the cohesive zone the stress state may be estimated by one of several available *cohesive zone models*. A simple example is the *Dugdale-Barenblatt* model that fixes the stress at a constant level taken to be the material's yield stress. Unfortunately, doing so also introduces an extra unknown in the form of the cohesive zone's extent. This, in turn, is found by invoking the additional requirement that at the crack tip the stress be finite. Finally, the requirement that energy released due to crack opening/closing equals the resulting increase/decrease in surface energy provides the equilibrated crack's length. Analogously [13], described the adhesive interaction between the punch and the half-space in terms of an "adhesive zone" of unknown extent that relieved the pressure's singularity obtained in the JKR approximation mentioned above. We will denote such models as *adhesive zone models*. The adhesive stresses were fixed at a known constant strength following the Dugdale-Barenblatt prescription. Finiteness of the contact pressure at the contact's boundary provided the adhesive zone's size, while the balance between the strain energy increase due to a growing contact and the accompanying decrease in surface energy allowed an estimate of the contact region's extent. Maugis [13] demonstrated that JKR and DMT approximations are contained within this more general framework. In particular, when the adhesive zone's size decreases to zero while the adhesive strength increases to infinity, we obtain the JKR approximation, while the limit of an infinite adhesive zone but vanishing adhesive strength coincides with the DMT approximation.

## 2. PROBLEM STATEMENT

The situation is shown in Fig. 1, where a rigid cylindrical punch of radius,  $R$ , is impressed upon an elastic and adhesive thin layer of thickness,  $b$ . A force,  $P$ , acts on the punch, leading to a vertical displacement,  $\delta$ , and contact over the region,  $[-a, a]$ . The thin layer's material is characterized by a Poisson's ratio,  $\nu$ , and Young's modulus,  $E$ . We assume that all approximations of Hertzian analysis hold, *viz.*, the contact zone's size,  $a \ll R$ , the vertical displacement,  $\delta \ll R$ , etc. Finally, the ratio  $b/a$  of the layer's height to the

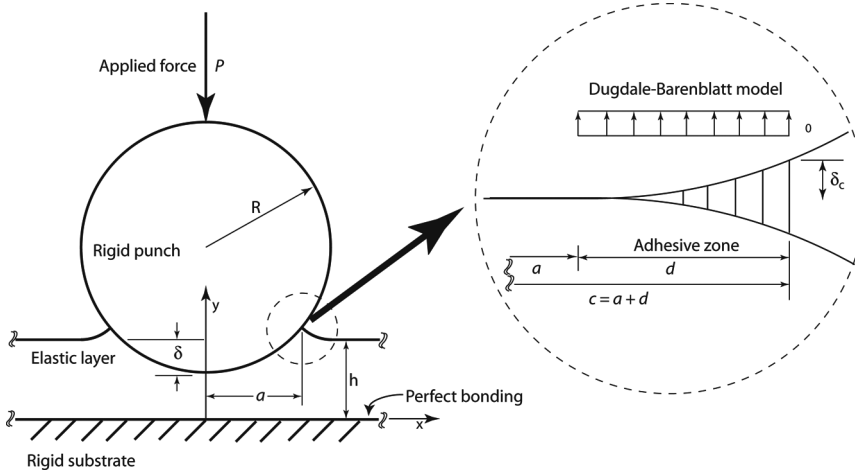


**FIGURE 1** Indentation of a cylindrical punch into an adhesive elastic layer. The adhesive zone along with the Dugdale-Barenblatt model is shown.

contact area, though quite small, cannot be arbitrarily small. This is because of technical difficulties in carrying out the approximate analysis of Sec. 3, and we will discuss this in a later section.

Outside the contact zone, adhesive forces act between the rigid punch and the elastic layer. These forces are assumed to act within a small *adhesive zone* of length,  $d$  (see Fig. 1), and are characterized by a constant strength,  $\sigma_0$ . This is, thus, a Dugdale-Barenblatt type model of the adhesive interaction. More complicated models such as the double-Hertz model ([18]), or one based on the Lennard-Jones potential are also possible, but we do not expect that this will introduce exceptional changes commensurate with the increased complexity.

### 3. ANALYSIS

#### 3.1. Governing Integral Equations

We will carry out a linear elastic analysis and, in keeping with Hertz's original assumption, we will reduce our contact problem to a mixed boundary-value problem for an elastic layer. From Fig. 1, we find the boundary conditions:

$$\text{At the substrate's interface, } i.e., y = 0: \quad u = 0, \quad v = 0 \quad (1a)$$

$$\text{On the layer's surface, } i.e., y = h: \quad \sigma_{xy} = 0,$$

$$\begin{cases} |x| > c: & \sigma_{yy} = 0, \\ a < |x| < c: & \sigma_{yy} = \sigma_0 \\ |x| < c: & v = -\delta + x^2/2R, \end{cases} \quad (1b)$$

where  $c = a + d$  locates the adhesive zone's edge. We immediately observe the mixed nature of the boundary conditions at  $y = b$ , where the normal stress is known outside the contact zone, while within that zone the layer must deform to accommodate the rigid punch's profile. We approximate the punch's cylindrical shape by the parabola  $y = -\delta + x^2/2R$  with its apex at  $x = y = 0$ . This is reasonable as long as  $\delta \ll R$ .

The equations of elasticity that must be satisfied are the Navier equations ([5], Sec. 1.10):

$$\frac{2(1-\nu)}{1-2\nu} \frac{\partial^2 u}{\partial x^2} + \frac{\partial^2 u}{\partial y^2} + \frac{1}{1-2\nu} \frac{\partial^2 v}{\partial x \partial y} = 0 \quad (2a)$$

and

$$\frac{2(1-\nu)}{1-2\nu} \frac{\partial^2 v}{\partial x^2} + \frac{\partial^2 v}{\partial y^2} + \frac{1}{1-2\nu} \frac{\partial^2 u}{\partial x \partial y} = 0 \quad (2b)$$

where we have assumed *plane strain* conditions as is appropriate for the contact of cylinders. The displacements  $u$  and  $v$  may be solved in terms of the unknown pressure  $p(x)$ <sup>1</sup> in the contact zone  $|x| < a$  by taking a Fourier transform in the  $x$ -direction of Eq. (2) and boundary conditions Eq. (1). Here we are interested in relating the known displacement boundary condition in  $|x| < a$  to the contact pressure,  $p(x)$ , therein. To this end, we will utilize integral transforms, see, e.g., [19]. We first find in Fourier space the vertical surface displacement, i.e.,  $V(\alpha, y)|_{y=b}$ :

$$V(\alpha) = \frac{2\tilde{P}(\alpha)}{E^* \alpha} \frac{2\kappa \sinh 2\alpha b - 4\alpha b}{2\kappa \cosh 2\alpha b + 4\alpha^2 b^2 + 1 + \kappa^2}, \quad (3)$$

where  $\alpha$  is the Fourier transform variable,  $\kappa = 3-4\nu$ ,  $E^* = E/(1-\nu^2)$ , and

$$\tilde{P}(\alpha) = -\frac{1}{2\pi} \int_{-\infty}^{\infty} \sigma_{yy}(t, b) e^{i\alpha t} dt \quad (4)$$

is the Fourier transform of the normal pressure on the elastic layer's upper surface. Taking the inverse Fourier transform of Eq. (3) and employing Eq. (4), we obtain the surface vertical displacement

$$v(x, y)|_{y=b} = v(x) = -\frac{1}{\pi E^*} \int_{-\infty}^{\infty} \frac{2\kappa \sinh 2\alpha b - 4\alpha b}{2\kappa \cosh 2\alpha b + 4\alpha^2 b^2 + 1 + \kappa^2} \frac{e^{-i\alpha x}}{\alpha} d\alpha \int_{-\infty}^{\infty} \sigma_{yy}(t, b) e^{i\alpha t} dt.$$

<sup>1</sup>Typically in contact mechanics the pressure on a surface is the negative of the normal stress acting on that surface. Thus,  $p(x) = -\sigma_{yy}|_{y=b}$ .

Changing the order of integration and recognizing from Eq. (1b) that  $\sigma_{yy}(t, b)$  vanishes for  $|t| > c$  and equals  $\sigma_0$  in the cohesive zone  $a < |t| < c$ , the above equation may be written as

$$v(x) = \frac{2}{\pi E^*} \left[ \sigma_0 \int_{-c}^{-a} \mathcal{K}(t-x) dt - \int_{-a}^a p(t) \mathcal{K}(t-x) dt + \sigma_0 \int_a^c \mathcal{K}(t-x) dt \right],$$

where, as mentioned before,  $p(t)$  is the unknown contact pressure, and the kernel

$$\mathcal{K}(s) = \int_0^\infty \frac{2\kappa \sinh 2\eta b - 4\eta b}{2\kappa \cosh 2\eta b + 4\eta^2 b^2 + 1 + \kappa^2} \frac{\cos s\eta}{\eta} d\eta. \quad (5)$$

The equation for the surface displacement may be rewritten as

$$v(x) = \frac{2}{\pi E^*} \left[ \sigma_0 \int_a^c \{ \mathcal{K}(t-x) + \mathcal{K}(t+x) \} dt - \int_{-a}^a p(t) \mathcal{K}(t-x) dt \right], \quad (6)$$

after a change of variables and noting that  $\mathcal{K}$  is a symmetric function. Restricting  $x$  to  $[-a, a]$ , so that the boundary condition in Eq. (1b) applies, we find that

$$-\delta + \frac{x^2}{2R} = \frac{2}{\pi E^*} \left[ \sigma_0 \int_a^c \{ \mathcal{K}(t-x) + \mathcal{K}(t+x) \} dt - \int_{-a}^a p(t) \mathcal{K}(t-x) dt \right], \quad (7)$$

$$-a \leq x \leq a.$$

If  $c$  was known, then so would be the integral over the adhesive zone  $[a, c]$  in the equation above, which will then represent an integral equation for the unknown contact pressure distribution,  $p(x)$ , with singular kernel,  $\mathcal{K}$ , given by Eq. (5).

As mentioned in the Introduction, we require enough closure equations to obtain a unique solution for the pressure distribution,  $p(x)$ , from the integral Eq. (7). The first of these notes simply that the total force applied on the punch balances the interaction with the elastic layer, *i.e.*,

$$P = \int_{-a}^a p(x) dx - 2\sigma_0(c-a). \quad (8)$$

Next, we recall that a reason to explicitly introduce an adhesive zone outside the contact region, in contrast to, say, the energy method of [8], was to relieve the stress singularity at the contact edge. Therefore, we must have

$$\lim_{x \rightarrow a^-} p(x) = p(a) \text{ is finite, } i.e., |p(a)| < \infty,$$

where we have written  $p(a)$  for what should technically be  $p(a^-)$ . However, because we restrict the nomenclature  $p(x)$  for the pressure distribution within

the contact zone, this, in a sense, is consistent. An equivalent, but more useful rephrasing of the above finiteness condition, at least in the context of our computation, is to require continuity of normal stress at  $x = a$ , *i.e.*,

$$\lim_{x \rightarrow a^-} p(x) = -\sigma_0 \quad (9)$$

if the vertical surface traction is discontinuous at the contact edge, the contact pressure cannot be finite. Finally, the last closure condition requires that the strain energy release rate balance the surface energy, *i.e.*,

$$\sigma_0 \delta_c = w, \quad (10)$$

where  $w$  is the *work of adhesion*, a material property, and the *air gap*

$$\delta_c = \frac{c^2}{2R} - \delta - v(c) \quad (11)$$

is the vertical distance of the punch's profile from the deformed layer's surface at the adhesive zone's edge, *i.e.*, at  $x = c$ . In fracture mechanics, this is termed the *crack opening displacement*; see also Fig. 1. Employing expression (6) at  $x = c$ , we find

$$v(c) = \frac{2}{\pi E^*} \left[ \sigma_0 \int_a^c \{ \mathcal{K}(t - c) + \mathcal{K}(t + c) \} dt - \int_{-a}^a p(t) \mathcal{K}(t - c) dt \right], \quad (12)$$

while setting  $x = 0$  in Eq. (7) yields

$$\delta = -\frac{2}{\pi E^*} \left[ 2\sigma_0 \int_a^c \mathcal{K}(t) dt - \int_{-a}^a p(t) \mathcal{K}(t) dt \right]. \quad (13)$$

We now have all the relevant equations in place and proceed to non-dimensionalization.

### 3.2. Non-Dimensionalization

We follow [13] to introduce the dimensionless variables

$$\Delta = \delta \left( \frac{K^2}{\pi^2 w^2 R} \right)^{1/3}, \quad A = a \left( \frac{K}{\pi w R^2} \right)^{1/3}, \quad \lambda = 2\sigma_0 \left( \frac{R}{\pi w K^2} \right)^{1/3}, \quad (14)$$

$$\bar{P} = \frac{P}{\pi w} \quad \text{and} \quad H = \frac{h}{R},$$

where  $K = \sqrt[3]{4E^*}$ , along with the internal scalings

$$\{ \xi, \tau, c_1 \} = \left\{ \frac{x}{a}, \frac{t}{a}, \frac{c}{a} \right\}, \quad \varphi = \frac{pa}{\pi w}, \quad m = \left( \frac{\pi w}{RK} \right)^{1/3} \quad \text{and} \quad \gamma = \frac{H}{mA}. \quad (15)$$

We also rewrite Eq. (5) as

$$\mathcal{K}(s) = \int_0^\infty \frac{\mathcal{A}(\omega)}{\omega} \cos s\omega \, d\omega \quad (16)$$

in terms of

$$\mathcal{A}(\omega) = \frac{2\kappa \sinh 2\omega - 4\omega}{2\kappa \cosh 2\omega + 4\omega^2 + 1 + \kappa^2}. \quad (17)$$

Employing the above in the equations developed in the previous section, we obtain the following four coupled non-dimensional equations:

$$\begin{aligned} \frac{\xi^2 A^2}{2} - \Delta &= \frac{4\lambda A}{3\pi} \{ \mathcal{J}^{(1)}(\xi) + \mathcal{J}^{(1)}(-\xi) \} \\ &- \frac{8m}{3\pi} \int_{-1}^1 \varphi(\tau) \mathcal{K}\left(\frac{\tau - \xi}{\gamma}\right) d\tau, \quad \text{for } -1 \leq \xi \leq 1 \end{aligned} \quad (18a)$$

$$\bar{P} = \int_{-1}^1 \varphi(\tau) d\tau - \frac{\lambda A}{m} (c_1 - 1), \quad (18b)$$

$$\lim_{\xi \rightarrow 1^-} \varphi(\xi) = \varphi(1) = -\frac{\lambda A}{2m} \quad (18c)$$

and

$$1 = \frac{\pi\lambda}{2} \left( \frac{c_1^2 A^2}{2} - \Delta - V(c_1) \right), \quad (18d)$$

where, we define

$$\mathcal{J}^{(\alpha)}(\xi) = \int_\alpha^{c_1} \mathcal{K}\left(\frac{\tau - \xi}{\gamma}\right) d\tau = \gamma \int_0^\infty \frac{\mathcal{A}(\omega)}{\omega^2} (\sin \chi_2 \omega - \sin \chi_1 \omega) d\omega, \quad (19)$$

with  $\chi_2 = (c_1 - \xi)/\gamma$  and  $\chi_1 = (\alpha - \xi)/\gamma$ , and note that the non-dimensionalized vertical displacements at the contact edge and the center-line are, respectively,

$$V(c_1) = \frac{4}{3\pi} \left[ \lambda A \{ \mathcal{J}^{(1)}(c_1) + \mathcal{J}^{(1)}(-c_1) \} - 2m \int_{-1}^1 \varphi(\tau) \mathcal{K}\left(\frac{\tau - c_1}{\gamma}\right) d\tau \right] \quad (20a)$$

and

$$\Delta = -\frac{8}{3\pi} \left[ \lambda A \int_1^{c_1} \mathcal{K}\left(\frac{\tau}{\gamma}\right) d\tau - m \int_{-1}^1 \varphi(\tau) \mathcal{K}\left(\frac{\tau}{\gamma}\right) d\tau \right] \quad (20b)$$

Given the system's material and geometric properties as captured by the parameter  $m$ , the above set of equations are to be solved for the unknown pressure distribution,  $\varphi$ , and the adhesive zone's extent,  $c_1$ . They will also provide relations between the center-line's vertical displacement,  $\Delta$ , the contact region's size,  $A$ , and the applied total force,  $\bar{P}$ .

### 3.3. Solution

We will seek to solve the set of Eqs. (18) approximately. To this end, we will expand the unknown  $\varphi$  in terms of a finite number of Chebyshev polynomials. These latter polynomials are chosen for their remarkable properties; see *e.g.*, [20] or [21]. It will then be possible to express Eqs. (18a), (18c), and (18d) as a set of non-linear algebraic equations in terms of the unknown coefficients in  $\varphi$ 's expansion,  $A$ ,  $\Delta$ , and  $c_1$ ; note  $\bar{P}$ 's absence in these three equations. The total applied force,  $\bar{P}$ , will be found directly from Eq. (18b). We observe that we obtain a set of non-linear equations because of the presence of an adhesive zone. In the absence of adhesion, *i.e.*, in the Hertz problem, this technique yields a linear algebraic system, see, *e.g.*, [5]. In fact, linearity persists even in the JKR approximation as we demonstrate in a later section. Reference [5] further notes that employing only the first six even Chebyshev polynomials yields very acceptable answers. This procedure will require us to evaluate the singular kernel,  $\mathcal{K}$ , given by Eq. (5) that, due to its complexity, may only be done numerically. To accomplish this successfully, it is necessary to first isolate  $\mathcal{K}$ 's singular part and estimate its contribution separately. This is done below.

In the sequel, we will often take recourse to numerical quadrature. To this end, we note two schemes. The *Gauss-Laguerre* method is useful for integration of exponentially decaying integrands over infinite domains, and yields the approximation

$$\int_0^\infty f(\omega)e^{-\omega}d\omega \approx \sum_{l=1}^n W_l f(\omega_l), \quad (21)$$

where  $f(\omega)$  is any function increasing at most polynomially at infinity,  $\omega_l$  is the  $l^{\text{th}}$ -root of the  $n^{\text{th}}$ -order Laguerre polynomial  $L_n(\omega)$ , and  $W_l$  are associated weights; see, *e.g.*, [22, p. 457]. In our computations, we take  $n = 64$ . Another numerical method that will be employed frequently is the *Gauss-Chebyshev* quadrature scheme under which

$$\int_{-1}^1 \frac{f(\tau)}{\sqrt{1-\tau^2}}d\tau \approx \frac{\pi}{M+1} \sum_{k=1}^{M+1} f(\tau_k), \quad (22)$$

where  $f(\tau)$  is a piecewise continuous function and

$$\tau_k = \cos \left[ \frac{(2k-1)\pi}{(M+1)2} \right] \quad (23)$$

are the roots of the Chebyshev polynomial  $T_{M+2}(\tau)$ ; see, e.g., [21, p. 180].

We will also need a nonlinear root-finding algorithm. Of the several available, we employ a bisection method because of its ease of implementation, specifically, the fact that derivatives are not required for updating the target root's value. While a good description is available in, say, [22, p. 62], a short summary of the algorithm is provided next. Suppose we wish to solve  $f(x) = 0$ , then we proceed as follows:

1. We choose an *interval of uncertainty*, say  $[a, b]$ , such that  $f(a)$  and  $f(b)$  are of opposite signs. If  $f$  is continuous, we are ensured that at least one root will lie within  $[a_1, a_2]$ .
2. Choose  $a_3 = (a_1 + a_2)/2$ .
3. Redefine the uncertainty interval as  $[a_1, a_3]$  or  $[a_3, a_2]$  depending on whether  $f(a_3)$ 's sign is the same as  $f(a_2)$  or  $f(a_1)$ , respectively.
4. Continue for either a specified number of iterations, or till some accuracy criterion is met. We employ the former choice here.

We note that the bisection method works best when there is only one root within the interval of uncertainty, and care is needed to ensure this.

For future use we also note the orthogonality property of Chebyshev polynomials

$$\int_{-1}^1 \frac{T_m(\tau)T_n(\tau)}{\sqrt{1-\tau^2}} d\tau = \begin{cases} \pi & \text{for } m = n = 0 \\ \pi/2 & \text{for } m = n \neq 0 \\ 0 & \text{for } m \neq n. \end{cases} \quad (24)$$

Finally, a comment on our solution's range of applicability. As [5] notes on p. 267, in the case of the non-adhesive contact of a rigid punch with an elastic layer, the present method breaks down when the layers are extremely thin. In our case this corresponds to  $H < 0.07$ . The reason for this breakdown lies in the inadequacy of a series of Chebyshev polynomials to approximate the pressure distribution for infinitesimally thin films.

### 3.3.1. Discretization and Computation

We approximate the unknown non-dimensionalized pressure distribution,  $\varphi(\xi)$ , as

$$\varphi(\xi) \approx -\frac{\lambda A}{2m} + \frac{1}{\sqrt{1-\xi^2}} \sum_{i=0}^N b_{2i} T_{2i}(\xi) \quad \text{for } -1 \leq \xi \leq 1. \quad (25)$$

The inverse square-root is made explicit in order to capture singular solutions such as the JKR approximation, and also to aid in applying the orthogonality property listed at the previous section's end. Furthermore, the leading constant term is included to better handle the continuity requirement [Eq. (18c)]. Finally, we have appealed to the punch's symmetry to retain only the even Chebyshev polynomials  $T_0, T_2, \dots, T_{2N}$ . We will now substitute the above expansion for  $\varphi$  into Eq. (18) to obtain algebraic equations in terms of  $b_{2i}, \Delta, \bar{P}, c_1$  and  $A$ . This will constitute an approximate solution to our problem. For Eq. (18c), we find for  $-1 \leq \xi \leq 1$ :

$$\left(\frac{A^2}{4} - \Delta\right) T_0(\xi) + \frac{A^2}{4} T_2(\xi) = \frac{4\lambda A}{3\pi} \{\mathcal{J}^{(0)}(\xi) + \mathcal{J}^{(0)}(-\xi)\} - \frac{8m}{3\pi} \sum_{i=0}^N b_{2i} \int_{-1}^1 \frac{T_{2i}(\tau)}{\sqrt{1-\tau^2}} \mathcal{K}\left(\frac{\tau-\xi}{\gamma}\right) d\tau,$$

where on the left hand side we have expanded  $\xi^2 A^2/2 - \Delta$  in terms of Chebyshev polynomials, while on the right side we have employed evenness of  $T_{2j}$  and  $\mathcal{K}$  to note that

$$\int_{-1}^1 \mathcal{K}\left(\frac{\tau-\xi}{\gamma}\right) d\tau = \int_0^1 \mathcal{K}\left(\frac{\tau-\xi}{\gamma}\right) d\tau + \int_0^1 \mathcal{K}\left(\frac{\tau+\xi}{\gamma}\right) d\tau,$$

so that the term stemming from the constant part of  $\varphi$  in Eq. (25) adds to  $\mathcal{J}^{(1)}(\xi) + \mathcal{J}^{(1)}(-\xi)$  yielding  $\mathcal{J}^{(0)}(\xi) + \mathcal{J}^{(0)}(-\xi)$ . The integral equation above is finally multiplied by  $T_{2j}(\xi)/\sqrt{1-\xi^2}$ , with  $j=0, \dots, N$ , and integrated over  $[-1, 1]$  to find the  $N+1$  equations

$$\begin{aligned} \left(\frac{A^2}{4} - \Delta\right) \pi &= \frac{8\lambda A}{3\pi} \tilde{\mathcal{J}}_0 - \frac{8m}{3\pi} \sum_{i=0}^N b_{2i} \tilde{\mathcal{K}}_{i0}, \quad \text{for } j=0, \\ \frac{A^2}{4} \frac{\pi}{2} &= \frac{8\lambda A}{3\pi} \tilde{\mathcal{J}}_1 - \frac{8m}{3\pi} \sum_{i=0}^N b_{2i} \tilde{\mathcal{K}}_{i1}, \quad \text{for } j=1, \end{aligned} \tag{26}$$

and

$$0 = \frac{8\lambda A}{3\pi} \tilde{\mathcal{J}}_j - \frac{8m}{3\pi} \sum_{i=0}^N b_{2i} \tilde{\mathcal{K}}_{ij}, \quad \text{for } j=2, \dots, N,$$

where we have employed the fact that, because  $T_{2i}(\xi) = T_{2i}(-\xi)$ ,

$$\int_{-1}^1 T_{2i}(\xi) \{\mathcal{J}^{(0)}(\xi) + \mathcal{J}^{(0)}(-\xi)\} d\xi = 2 \int_{-1}^1 T_{2i}(\xi) \mathcal{J}^{(0)}(\xi) d\xi$$

and defined the projections

$$\tilde{\mathcal{J}}_j = \int_{-1}^1 \frac{T_{2j}(\xi)}{\sqrt{1-\xi^2}} \mathcal{J}^{(0)}(\xi) d\xi \quad (27a)$$

and

$$\tilde{\mathcal{K}}_{ij} = \int_{-1}^1 \int_{-1}^1 \frac{T_{2j}(\xi) T_{2i}(\tau)}{\sqrt{1-\xi^2} \sqrt{1-\tau^2}} \mathcal{K}\left(\frac{\tau-\xi}{\gamma}\right) d\tau d\xi \quad (27b)$$

of  $\mathcal{J}^{(0)}(\xi)$  and  $\mathcal{K}[(\tau-\xi)/\gamma]$  onto single and double Chebyshev series, respectively. However, in order to compute these projections we need to isolate any singularities that  $\mathcal{K}$  may have.

We note from Eq. (17) that, as  $\omega \rightarrow \infty$ ,  $\mathcal{A}(\omega) \rightarrow 1$  and, consequently, from Eq. (16),  $\mathcal{K}$  would have had a logarithmic singularity at infinity but for the cosine term's increasingly fast oscillations as  $\omega$  grows. Nevertheless,  $\mathcal{K}'$ 's value is dominated by  $\mathcal{A}'$ 's asymptotic behavior for large  $\omega$ . We extract this singularity by adding and subtracting from  $\mathcal{A}(\omega)$  the term  $1 - \exp(-q\omega)$ , where  $q > 0$ . Note that the exponential term is introduced to allow the resulting cosine transform to exist; any positive and finite  $q$  may be employed. Utilizing the Fourier cosine transform tables [23, p. 1118], we then write

$$\begin{aligned} \mathcal{K}(s) = & -\ln|s| + \ln\sqrt{s^2 + q^2} + \int_0^\infty \frac{1}{\omega} \{A(\omega) - 1 + e^{-q\omega}\} \cos s\omega d\omega =: \\ & -\ln|s| + \mathcal{F}(s), \end{aligned} \quad (28)$$

where the integral contained in  $\mathcal{F}$  is now a regular Fourier cosine transform and, though still analytically intractable, is easily evaluated numerically for any  $q > 1$  by, say, the Gauss-Laguerre scheme mentioned previously. This yields

$$\mathcal{F}(s) \approx \ln\sqrt{s^2 + q^2} + \sum_{l=1}^n W_l e^{\omega_l} \{A(\omega_l) - 1 + e^{-q\omega_l}\} \frac{\cos s\omega_l}{\omega_l}. \quad (29)$$

From the nature of  $\mathcal{K}'$ 's singularity, we observe that  $\mathcal{J}^{(0)}$  is not singular for  $0 \leq \xi \leq 1$ , so that  $\tilde{\mathcal{J}}_j$  is easily found by Gauss-Chebyshev quadrature:

$$\tilde{\mathcal{J}}_j \approx \frac{1}{M+1} \sum_{k=1}^M T_{2j}(\xi_k) \mathcal{J}^{(0)}(\xi_k), \quad (30)$$

where  $\xi_k$  are the roots of  $T_{M+2}(\xi)$  and given by Eq. (23), while  $\mathcal{J}^{(0)}(\xi_k)$  are obtained after setting  $\alpha = 0$  in Eq. (19) and applying Gauss-Laguerre

quadrature:

$$\mathcal{J}^{(0)}(\xi_k) \approx \gamma \sum_{l=1}^n W_l e^{\omega_l} \{ \mathcal{A}(\omega_l) - 1 + e^{-q\omega_l} \} \frac{\sin(c_1 - \xi_k)\omega_l + \sin \xi_k \omega_l}{\omega_l^2}. \quad (31)$$

Evaluating  $\mathcal{K}_{ij}$  is trickier because of the presence of the logarithmic singularity in Eq. (28). Noting from [5, problem 8 on p. 69] or [24] that

$$\int_{-1}^1 \frac{T_{2i}(\tau) \ln \left| \frac{\tau - \xi}{\gamma} \right| d\tau = \begin{cases} \pi T_{2i}(\xi)/2i & \text{if } i \leq 1 \\ -\pi \ln(2\gamma) & \text{if } i = 0 \end{cases}$$

and invoking Eq. (24) allows us to write

$$\tilde{\mathcal{K}}_{ij} = \tilde{\mathcal{F}}_{ij} + \begin{cases} \pi^2/4j & \text{if } i = j \leq 1 \\ \pi^2 \ln(2\gamma) & \text{if } i = j = 0 \\ 0 & \text{if } i \neq j, \end{cases} \quad (32)$$

where repeated Gauss-Chebyshev quadrature yields

$$\tilde{\mathcal{F}}_{ij} = \frac{\pi^2}{(M+1)^2} \sum_{l=1}^{M+1} \sum_{k=1}^{M+1} T_{2j}(\xi_l) T_{2i}(\tau_k) \mathcal{F} \left( \frac{\tau_k - \xi_l}{\gamma} \right) \quad (33)$$

with  $\tau_k$  and  $\xi_l$  being the  $k$ th and  $l$ th roots of  $T_{M+1}$ , respectively, and  $\mathcal{F}$  may be evaluated from Eq. (29) with  $s = (\tau_k - \xi_l)/\gamma$ . We finally rewrite Eq. (26) as

$$\Delta = \frac{A^2}{4} - \frac{8\lambda A}{3\pi^2} \tilde{\mathcal{J}}_0 + \frac{8m}{3\pi^2} \sum_{i=0}^N b_{2i} \tilde{\mathcal{K}}_{i0}, \quad \text{for } j = 0 \quad (34a)$$

$$\sum_{i=0}^N b_{2i} \tilde{\mathcal{K}}_{i1} = \frac{\lambda A}{m} \tilde{\mathcal{J}}_1 - \frac{3\pi^2 A^2}{64m}, \quad \text{for } j = 1 \quad (34b)$$

and

$$\sum_{i=0}^N b_{2i} \tilde{\mathcal{K}}_{ij} = \frac{\lambda A}{m} \tilde{\mathcal{J}}_j, \quad \text{for } j = 2, \dots, N, \quad (34c)$$

with  $\tilde{\mathcal{J}}_j$  and  $\tilde{\mathcal{K}}_{ij}$  found from Eqs. (30) and (32), respectively. The above set of equations is the appropriate discretization of the integral Eq. (18a).

Similarly, utilizing Eq. (24) for  $m = n = 0$ , the discretization of Eq. (18b) is

$$\bar{P} = \pi b_0 - \frac{\lambda A}{m} c_1. \quad (35)$$

The continuity requirement [Eq. (18c)] is satisfied if we enforce

$$\sum_{i=1}^N b_{2i} = b_0 + b_2 + \dots + b_{2N} = 0. \quad (36)$$

Finally, the energy balance [Eq. (18c)] is rewritten as

$$\frac{\pi\lambda}{2} \left( \frac{c_1^2 A^2}{2} - \Delta - V(c_1) \right) - 1 = 0 \quad (37)$$

with  $\Delta$  given by Eq. (34a) and

$$V(c_1) = \frac{4\lambda A}{3\pi} \{ \tilde{\mathcal{F}}^{(0)}(c_1) + \tilde{\mathcal{F}}^{(0)}(-c_1) \} - \frac{8m}{3\pi} \sum_{i=0}^N b_{2i} \tilde{\mathcal{K}}_i(c_1), \quad (38)$$

where, with  $\tau_k$  given by Eq. (23),  $\mathcal{K}[(\tau - c_1)/\gamma]$ 's projection onto a Chebyshev basis are

$$\tilde{\mathcal{K}}_i(c_1) = \int_{-1}^1 \frac{T_{2i}(\tau)}{\sqrt{1-\tau^2}} \mathcal{K}\left(\frac{\tau - c_1}{\gamma}\right) d\tau \approx \frac{\pi}{M+1} \sum_{k=1}^{M+1} T_{2i}(\tau_k) \mathcal{K}\left(\frac{\tau_k - c_1}{\gamma}\right).$$

We note that we can alternatively employ a discretized version of Eq. (20b) to obtain  $\Delta$ .

For any fixed contact region size,  $A$ , Eqs. (34)–(37) represent  $N+4$  equations for the  $N+4$  unknowns  $b_{2i}$ ,  $\Delta$ ,  $\bar{P}$ , and  $c_1$ . Further, we note that Eq. (35) for  $\bar{P}$  is decoupled from the rest, in the sense that if  $c_1$  and  $b_0$  were known  $\bar{P}$  can be found. At the same time, if we assume  $c_1$  to be known, the  $N+2$  Eqs. (34) are simply linear algebraic equations for the coefficients  $b_{2i}$ . The choice of  $c_1$  is to be regulated by the satisfaction of Eq. (37) once  $\Delta$  is obtained from Eq. (34a). Our solution algorithm based on the bisection method described earlier is as follows:

1. Fix  $A$ . Assume an interval of uncertainty for  $c_1$ . For our choice of parameters, we typically employed [1.01, 100].
2. Solve Eqs. (34b)–(34c) and Eq. (36) for the  $b_{2i}$ .
3. Compute  $\Delta$  from Eq. (34a).
4. Employ the error in satisfying Eq. (37) to update the uncertainty interval.
5. Repeat for a specified number of iterations. We employ 20 iterations.
6. Employ the final values of  $c_1$  and  $b_{2i}$  to compute  $\bar{P}$  from Eq. (35) and stop.

In passing, note that we have only computed  $b_{2i}$ ,  $\Delta$ ,  $\bar{P}$ , and  $c_1$  by fixing  $A$  as it is the most convenient solution procedure. There is no experimental expediency for this choice.

## 4. RESULTS

Rather than proceeding directly to the results of the full problem, we will first put forward results for the Hertzian indentation of an elastic layer and for adhesive indentation investigated within the JKR approximation. While the former set of results are included mostly for completeness and to build confidence in our computations, the latter results are new. All through, we set the parameter  $m=0.0168$ , which, *e.g.*, corresponds to an adhesive elastic layer with  $w=0.02\text{J}$ ,  $E=0.083\text{MPa}$ , and  $\nu=0.4$ , and an indenter with  $R=10\text{cm}$ . Furthermore, we approximate the contact pressure distribution,  $\varphi$ , by the first six even Chebyshev polynomials, *i.e.*,  $N=6$ .

### 4.1. Elastic Non-Adhesive Contact: Hertz Problem

In the case of Hertzian contact, adhesion is absent and there is no adhesive zone. Thus,  $c_1=1$  and the energy balance [Eq. (10)] is redundant. For any value of  $A$ , we solve for the  $b_{2i}$  from Eqs. (34b) and (34c). This yields the contact pressure distribution,  $\varphi$ . The thus computed  $b_{2i}$  are employed to obtain  $\Delta$  from Eq. (34a) and  $\bar{P}$  from Eq. (35). The results<sup>2</sup> are shown in Figs. 2–5 for various elastic layer thicknesses  $H$ . Also shown by a line with dots are the solutions obtained for a two-dimensional half-space, *i.e.*,  $H=\infty$ , in which case the exact non-dimensional solutions are

$$\varphi(\xi) = \frac{3A^2}{8m} \sqrt{1 - \xi^2} \quad (39a)$$

$$\bar{P} = \frac{3\pi A^2}{16m} \quad (39b)$$

and

$$\Delta = \frac{A^2}{4} \left\{ 2 \ln \left( \frac{2d}{a} \right) - \frac{\nu}{1 - \nu} \right\} \quad (39c)$$

where  $d$  locates a reference point below the indenter's apex. The first two equations above are standard, see, *e.g.*, [25, p. 55], but a comment is in order regarding  $\Delta$ 's expression. It is well known that displacements are not obtained accurately in two-dimensional half-space problems, and, in fact,

---

<sup>2</sup>In Hertzian contact,  $w=\sigma_0=0$ . This would indicate that the non-dimensionalization introduced in Sec. 3.2 breaks down. However, rather than introducing new non-dimensionalization, we will, in the case of Hertzian contact, regard  $w$  employed in Eqs. (14) and (15) as an arbitrary scale and *not* as the work of adhesion.

display logarithmic growth as we move away from where forces are applied towards infinity, thereby making St. Venant's principle inapplicable. In two dimensions, the contacting bodies' finite geometry and the nature of their supports must be taken into account, and we refer the interested reader to the discussion in [15, Sec. 5.6]. Page 131 [15] provides the displacement,  $\Delta$ , of the center line *relative* to a point at a finite distance,  $d$ , away as given above, which does indeed display logarithmic growth as  $d \rightarrow \infty$ . When comparing our results for elastic layers with large  $H$  against solutions for a half-space, we will select  $d = H$  in  $\Delta$ 's formula. Note that the match will only be approximate, because, in contrast to the elastic layer, the displacement in a half-space at a point a distance  $H$  below the indenter's apex does *not* vanish.

We observe from Fig. 2 that the pressure distributions reduce continuously in magnitude. Similarly, from Fig. 3 we see that the applied load,  $\bar{P}$ , required to achieve the same contact region size,  $A$ , increases with decreasing layer thickness,  $H$ . The same is the case, if the control parameter was the center-line's vertical displacement,  $\Delta$ ; see Fig. 4. Similarly, in Fig. 5, the same  $\bar{P}$  leads to greater  $\Delta$  as the layer's thickness grows. These are expected behaviors, as the effective rigidity of the combined layer and rigid substrate system increases as the layer becomes thinner. Finally, as  $H \rightarrow 10$ , there is little to distinguish the system from an infinite half-space.

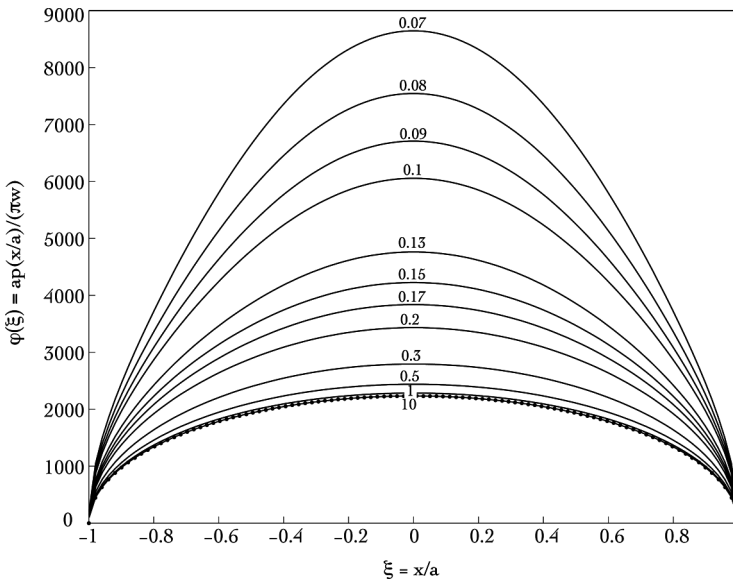


**FIGURE 2** Indentation of a non-adhesive cylindrical punch on an elastic layer. Variation of the non-dimensionalized pressure distribution,  $\varphi$ , within the contact region for  $A = 10$ . Several values of the layer's thickness,  $H$ , are investigated and the associated curves are appropriately indicated.

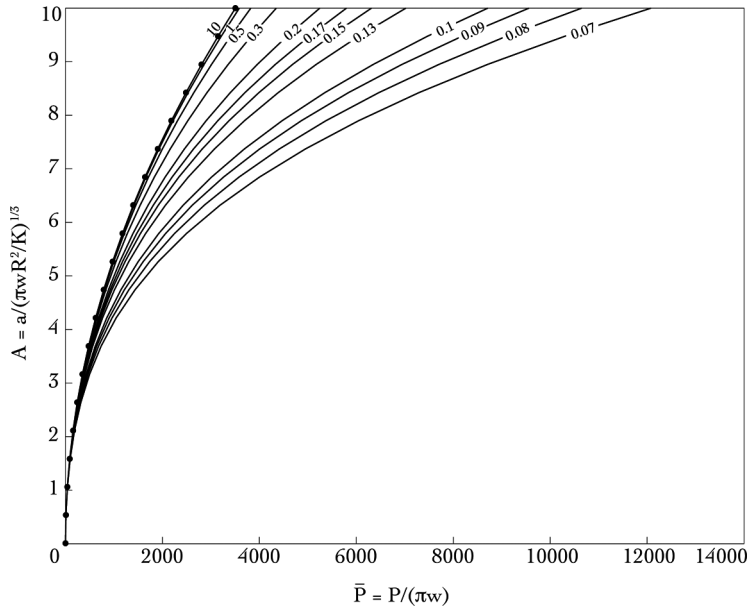


**FIGURE 3** Indentation of a non-adhesive cylindrical punch on an elastic layer. Variation of the contact region's non-dimensionalized size,  $A$ , is shown as a function of the scaled total force,  $\bar{P}$ . Several values of the layer's thickness,  $H$ , are investigated and the associated curves are appropriately indicated.

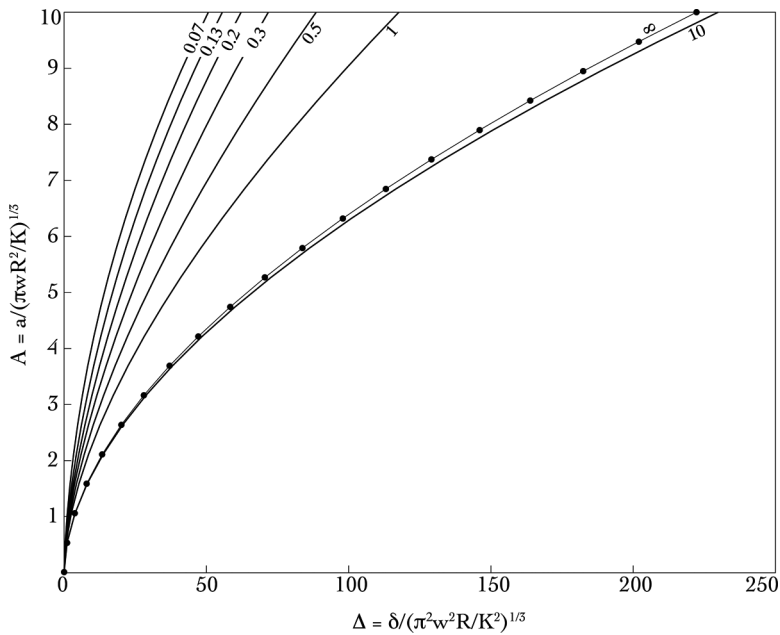


**FIGURE 4** Variation of the contact region's non-dimensionalized size,  $A$ , with the center-line's scaled vertical displacement,  $\Delta$ ; *cf.* caption of Fig. 3.

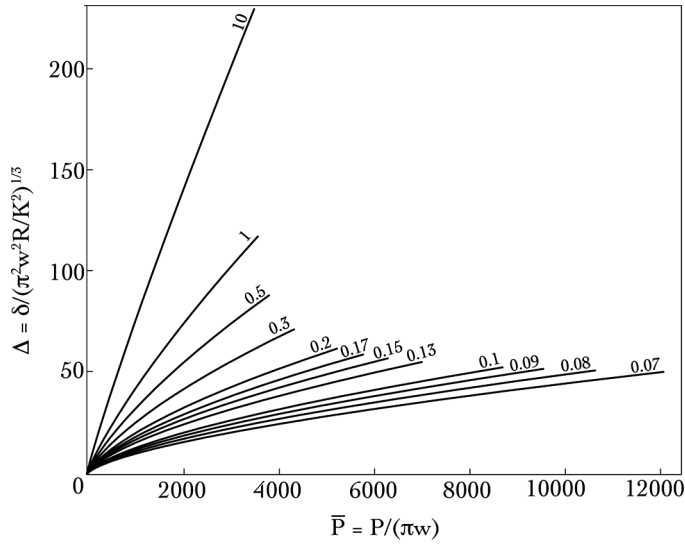


**FIGURE 5** Variation of the non-dimensionalized center-line's vertical displacement,  $\Delta$ , with the scaled total force,  $\bar{P}$ ; cf. caption of Fig. 3.

#### 4.2. Adhesive Contact: JKR Approximation

As mentioned earlier, the JKR approximation models adhesion by allowing the possibility of tensile stresses in the contact edge's vicinity. Furthermore, because adhesive interaction is precluded outside the contact region, the contact pressure distribution is found to be singular at the contact's edge. In this case, as [13] shows, the energy balance [Eq. (10)] reduces to the familiar Griffith's criterion in fracture mechanics ([17]), *i.e.*,

$$\frac{K_I^2}{2E^*} = w,$$

where

$$K_I = - \lim_{x \rightarrow a^-} \sqrt{2\pi(a-x)p(x)}$$

is the *stress intensity factor* that measures the intensity of the square root singularity at the contact's edge. Combining and non-dimensionalizing the above two equations, and observing the contact pressure distribution  $\varphi$ 's expansion [Eq. (25)], we find the relation

$$\sum_{i=0}^N b_{2i} = - \frac{\sqrt{6A}}{2\pi m} \quad (40)$$

that replaces the requirement [Eq. (36)]. Note that the non-vanishing negative right side above ensures that the contact pressure distribution is tensile near the contact's edge, and increases to infinity as the edge is approached. This singular feature is the primary drawback of the JKR approximation, and motivates the more physical model introduced by [13] and employed in the current work, *cf.*, Section 4.3.

The contact pressure distribution and the total contact force estimated by the JKR approximation for the adhesive contact of a cylinder on a half-space are, respectively,

$$\varphi(\xi) = \frac{3A^2}{8m} \sqrt{1 - \xi^2} - \frac{\sqrt{6A}}{2\pi m} \frac{1}{\sqrt{1 - \xi^2}} \quad (41a)$$

and

$$\bar{P} = \frac{3\pi A^2}{16m} - \frac{\sqrt{6A}}{2m}. \quad (41b)$$

The above exact results are represented by lines with black dots in Figs. 6 and 7 that display the contact pressure distribution and the relation between

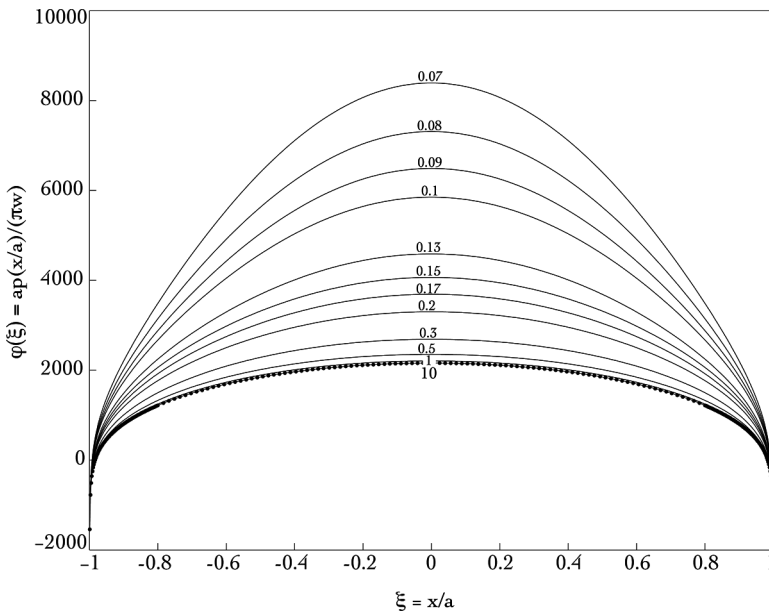


**FIGURE 6** Indentation of an adhesive cylindrical punch on an elastic layer: JKR approximation. Variation of the non-dimensionalized pressure distribution,  $\varphi$ , within the contact region for  $A = 10$ . Several values of the layer's thickness,  $H$ , are investigated and the associated curves are appropriately indicated.

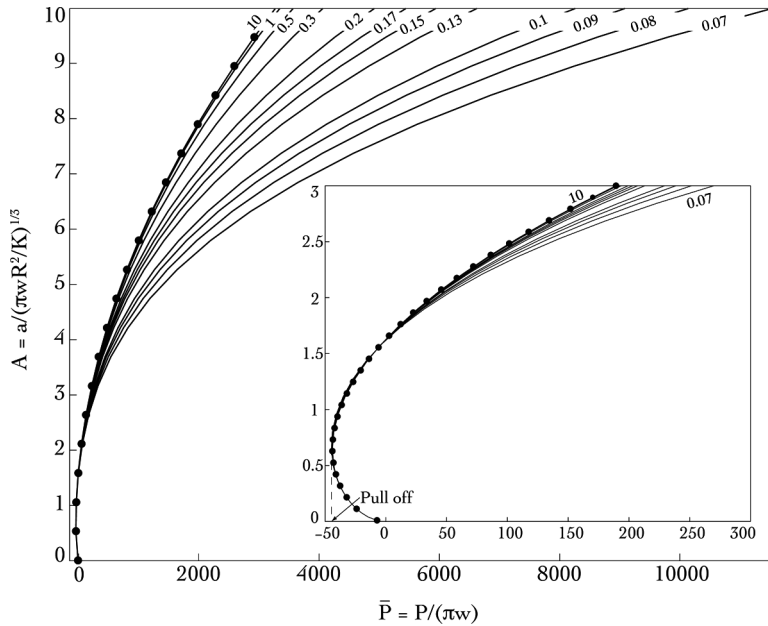


**FIGURE 7** Indentation of an adhesive cylindrical punch on an elastic layer: JKR approximation. Variation of the contact region's non-dimensionalized size,  $A$ , with the scaled total force  $\bar{P}$ . Several values of the layer's thickness,  $H$ , are investigated and the associated curves are appropriately indicated.

the contact region's size,  $A$ , and total load,  $\bar{P}$ , respectively. The inset in Fig. 7 shows the behavior over smaller contact areas. We observe from Fig. 6 that in keeping with the discussion in the previous paragraph, the pressure becomes tensile near the contact edge, and grows unboundedly as the edge is approached. Furthermore, from Fig. 7 we note that due to the presence of adhesive interaction, a negative  $\bar{P}$  is required to detach the punch. Similarly, contact is initiated even while  $\bar{P}$  vanishes. However, as the inset in Fig. 7 suggests, the pull-off force changes little with the layer's thickness. We also observe that as  $H \rightarrow 10$  we recover the half-space ( $H \rightarrow \infty$ ) JKR solution. Finally, we also plot in Figs. 8 and 9 the variation of  $A$  with the center-line's vertical displacement,  $\Delta$ , and of  $\Delta$  with the total load,  $\bar{P}$ , respectively.

#### 4.3. Adhesive Contact: Adhesive Zone Model

We return finally to our original model, wherein singularities in the contact pressure are removed by the physical mechanism of an adhesive zone extending beyond the contact region. The analytical expressions for the contact pressure distribution and the total load in the case of a half-space ( $H \rightarrow \infty$ ) while including an adhesive zone may be

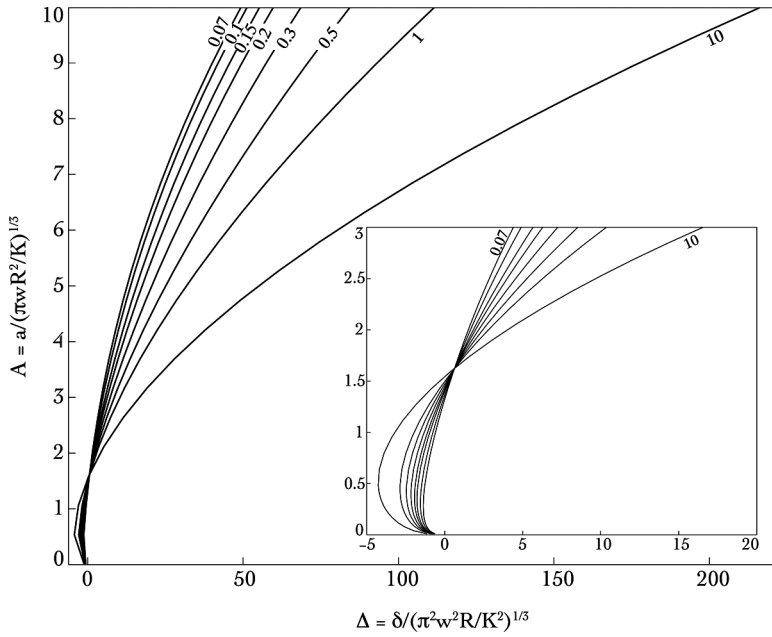


**FIGURE 8** Variation of the contact region's non-dimensionalized size,  $A$ , with the center-line's scaled vertical displacement,  $\Delta$ ; *cf.* caption of Fig. 7.

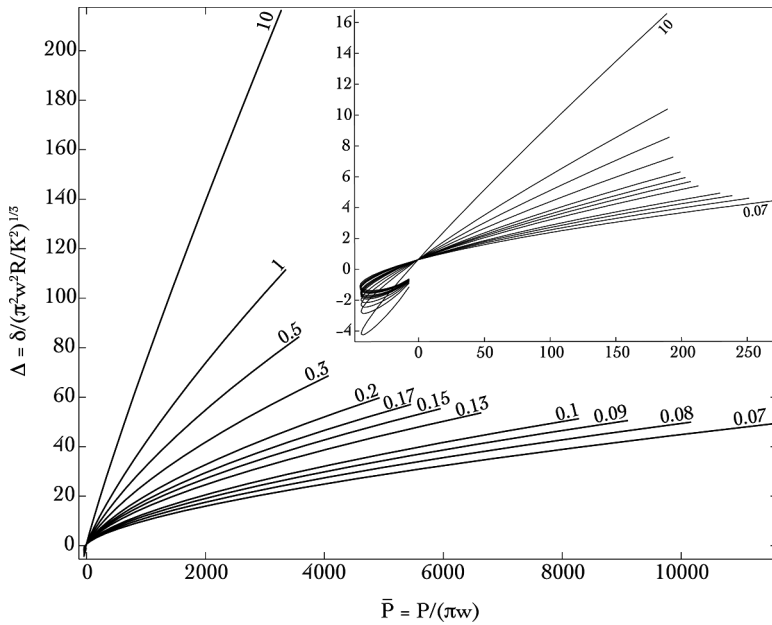


**FIGURE 9** Variation of the non-dimensionalized center-line's vertical displacement,  $\Delta$ , with the scaled total force,  $\bar{P}$ ; *cf.* caption of Fig. 7.

obtained [26]. We find that

$$\varphi(\xi) = \frac{3A^2}{8m} \sqrt{1 - \xi^2} - \frac{A\lambda}{\pi m} \tan^{-1} \sqrt{\frac{c_1^2 - 1}{1 - \xi^2}} \quad (42a)$$

and

$$\bar{P} = \frac{3\pi A^2}{16m} - \frac{A\lambda}{m} \sqrt{c_1^2 - 1}, \quad (42b)$$

where the adhesive zone's extent,  $c_1$ , is obtained by the solution of a pair of nonlinear algebraic equations; [26, Eqs. (22) and (23)]. However, rather than seek a solution to these latter two equations when comparing our results for large  $H$  with the formulae above, we employ the adhesive zone lengths,  $c_1$ , as computed by us. This may lead to slight errors, and indeed it does, in the case when  $\lambda$  is large, as then the adhesive zone's length,  $d_1$ , is small (see Fig. 17), so that small relative differences in computing  $c_1$  leads to comparatively greater errors.

The pressure profiles for  $A = 3$  are shown in Fig. 10. It is confirmed that the pressure is continuous at the contact edge. We also note that the pressure

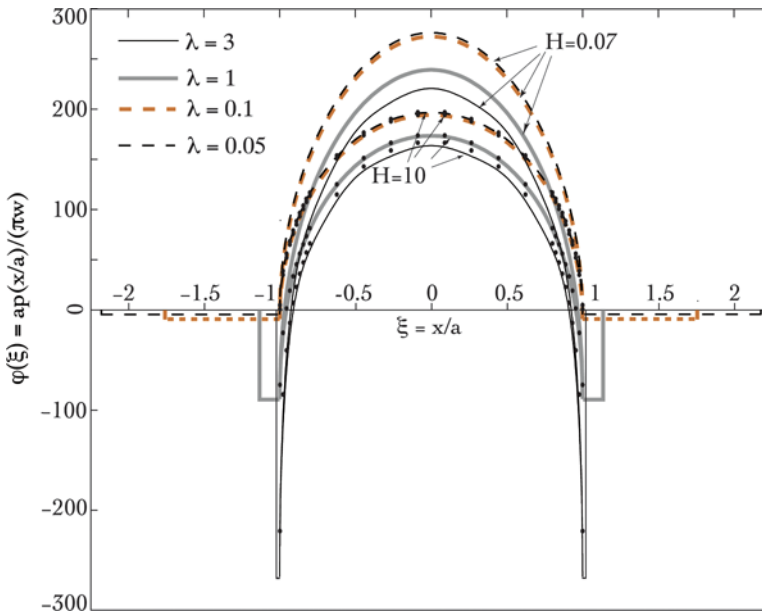


**FIGURE 10** Indentation of an adhesive cylindrical punch on an elastic layer: Adhesive zone model. Variation of the non-dimensionalized pressure distribution,  $\varphi$ , within the contact region for  $A = 3$ . Two extreme values of the layer's thickness,  $H$ , are investigated, along with four different choices of  $\lambda$  (color figure available online).

become tensile (negative) near the contact edge and increases sharply until it saturates at the adhesive stress' value of  $-\lambda A/2m$ . As  $\lambda$  increases, the adhesive zone decreases, but the adhesive stress level increases, so that in

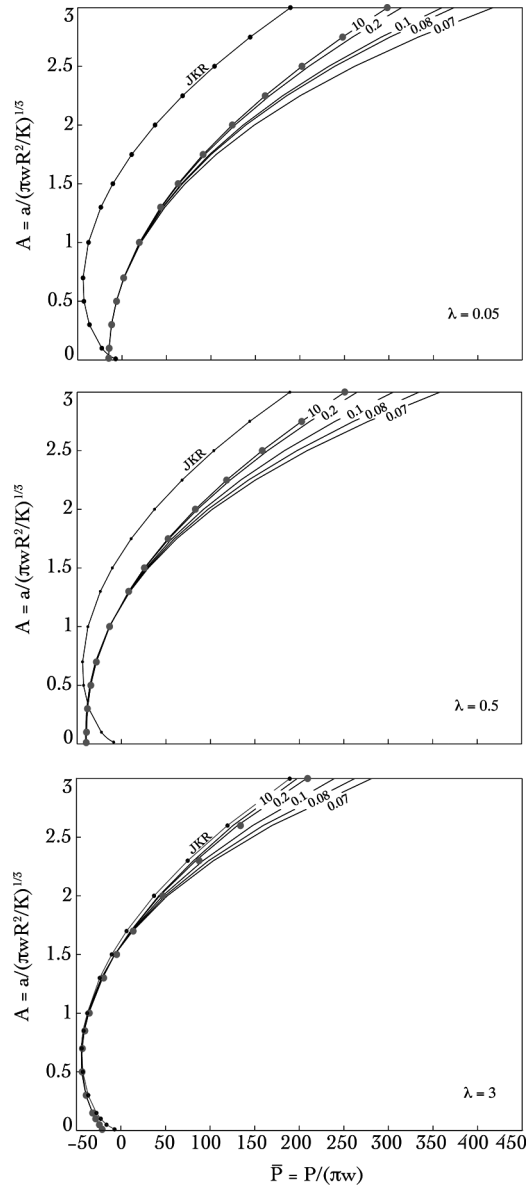


**FIGURE 11** Indentation of an adhesive cylindrical punch on an elastic layer for various  $\lambda$ 's. Variation of the contact region's non-dimensionalized size,  $A$ , is shown as a function of the scaled total force,  $\bar{P}$ . Several values of the layer's thickness,  $H$ , are investigated and the associated curves are appropriately indicated.

the limit  $\lambda \rightarrow \infty$ , we have infinite adhesive stresses spread over a vanishingly small adhesive zone; *cf.* Fig. 17. We also observe that, as before, the thinner layer is stiffer, so that the pressure is greater. Predictions given above for the case of a half-space are represented by black dots for the four choices of  $\lambda$ . As expected, for all choices of the adhesive strength,  $\lambda$ , there is very

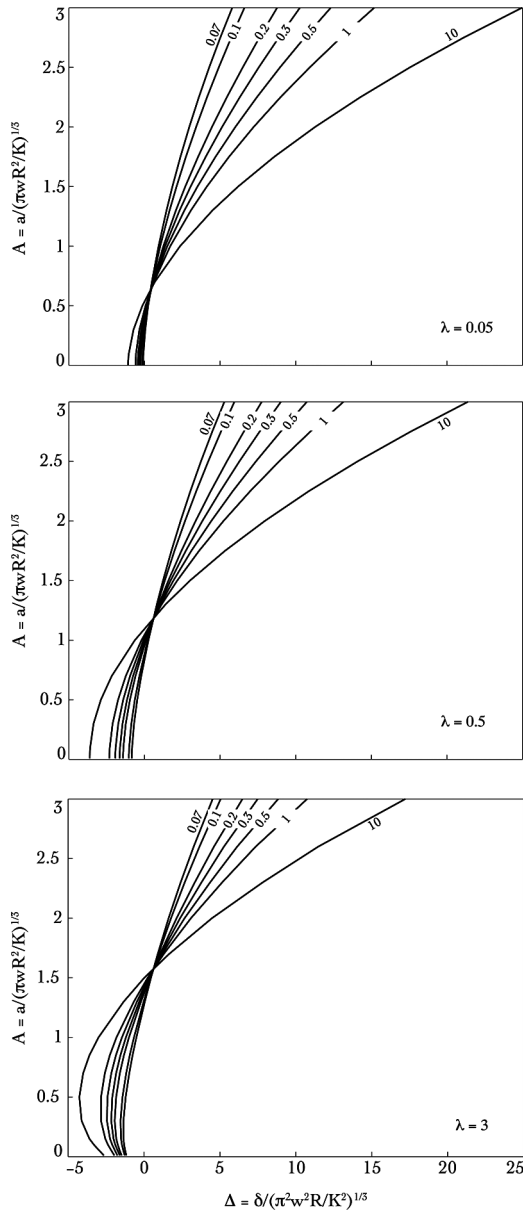


**FIGURE 12** Variation of the contact region's non-dimensionalized size,  $A$ , with the center-line's scaled vertical displacement,  $\Delta$ ; *cf.* caption of Fig. 11.

close match when  $H=10$ . The slight mismatch when  $\lambda=3$  is for reasons noted previously.

We next explore relationships between the three focal parameters, the contact region's size,  $A$ , the total load,  $\bar{P}$ , and the center-line's displacement,  $\Delta$ , for various values of the elastic layer's thickness,  $H$ , and adhesive strength,  $\lambda$ . Figures 11–16 report the results. Figure 11 plots the variation of the contact

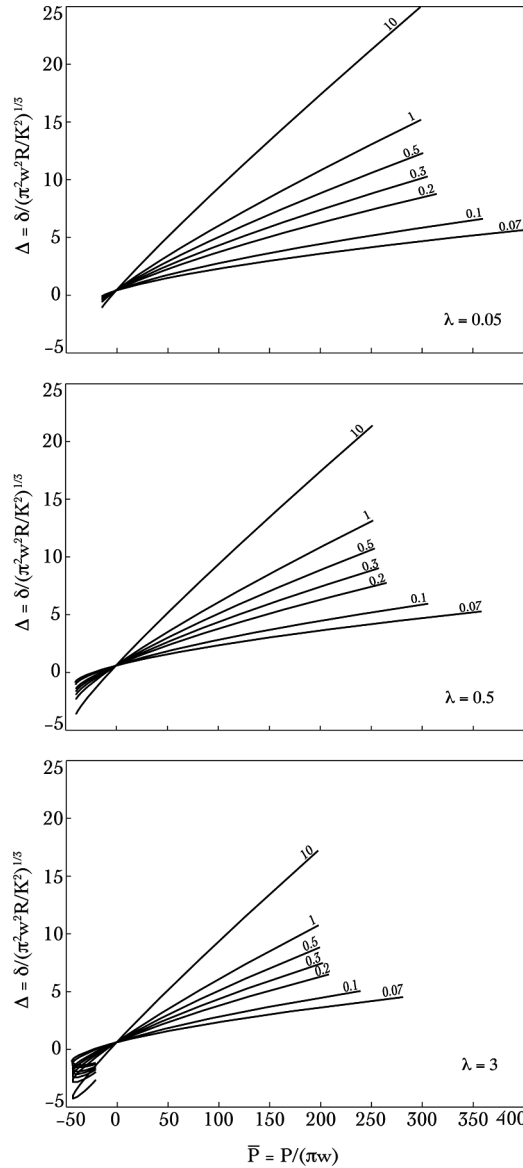


**FIGURE 13** Variation of the non-dimensionalized center-line's vertical displacement,  $\Delta$ , with the scaled total force,  $\bar{P}$ ; cf. caption of Fig. 11.

region's size,  $A$ , against the total load,  $\bar{P}$ , for various layer thicknesses,  $H$ . Three different values of the adhesive strength,  $\lambda$ , are investigated. Also shown by a black dotted line is the JKR approximation for a half-space,

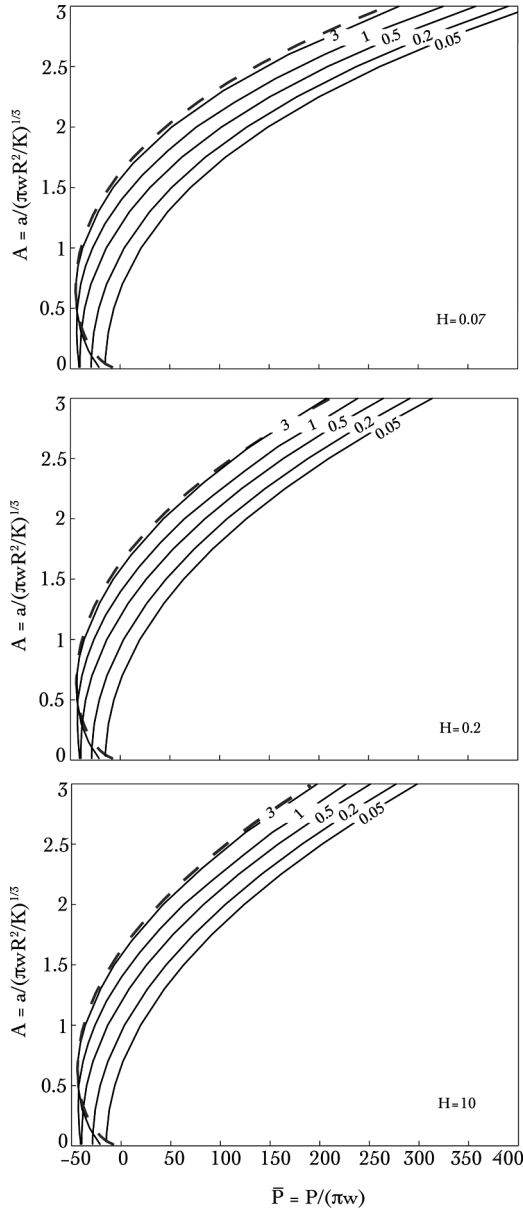


**FIGURE 14** Indentation of an adhesive cylindrical punch on an elastic layer for various adhesive strengths,  $\lambda$ . Variation of the contact region's non-dimensionalized size,  $A$ , is shown as a function of the scaled total force,  $\bar{P}$ . Several values of the adhesion parameter,  $\lambda$ , are investigated and the associated curves are appropriately indicated.

*i.e.*, a layer of infinite thickness. Finally, the analytical result for a half-space listed above is shown by large gray-filled circles. We see that the JKR approximation matches the curve due to  $H=10$  very closely at the high  $\lambda$

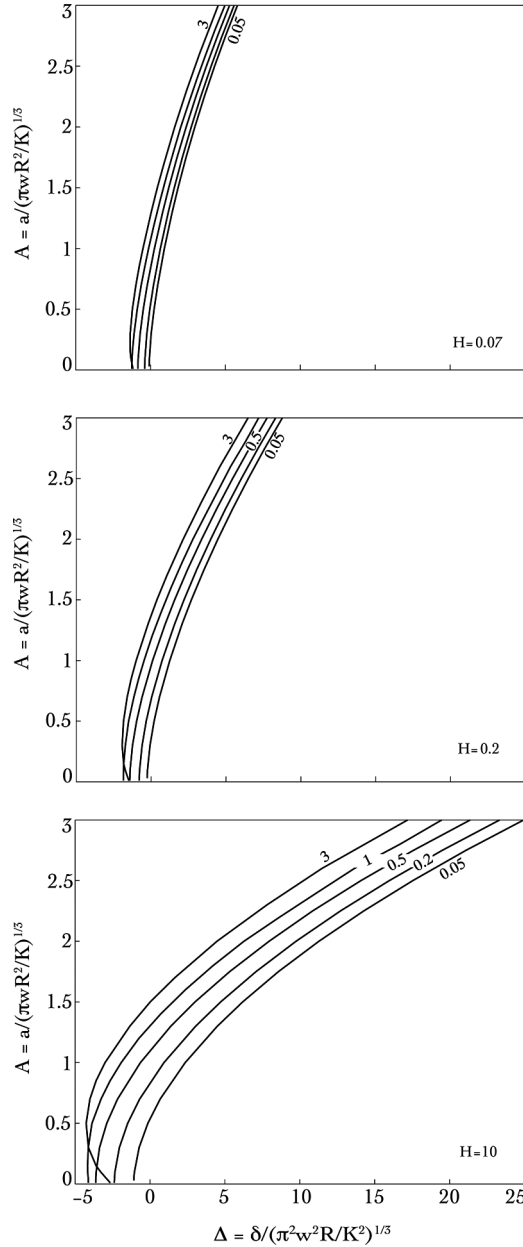


**FIGURE 15** Variation of the contact region's non-dimensionalized size,  $A$ , with the center-line's scaled vertical displacement,  $\Delta$ ; *cf.* caption of Fig. 14.

of 3. As expected, the match deteriorates as  $\lambda$  decreases. Similarly, the exact formulae for an adhesive zone model in the case of a half-space agrees very well with our computed results when  $H \rightarrow 10$ . Again, the match is slightly off when  $\lambda = 3$  for reasons mentioned above.

Figures 12 and 13 plot variation of  $A$  with center-line displacement  $\Delta$ , and  $\Delta$  against the total pressure,  $\bar{P}$ , at various  $H$  for three different  $\lambda$ 's. We observe that at a fixed  $\Delta$ , smaller contact regions are obtained when the adhesive strength,  $\lambda$ , is lower. Similarly, larger pull-off forces/displacements are required when  $\lambda$  is large.

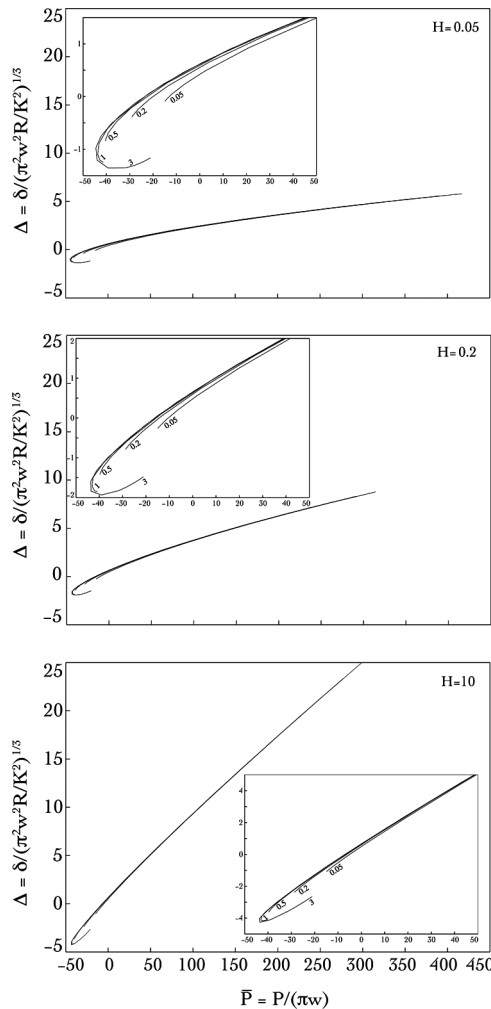


**FIGURE 16** Variation of the non-dimensionalized center-line's vertical displacement,  $\Delta$ , with the scaled total force,  $\bar{P}$ ; cf. caption of Fig. 14.

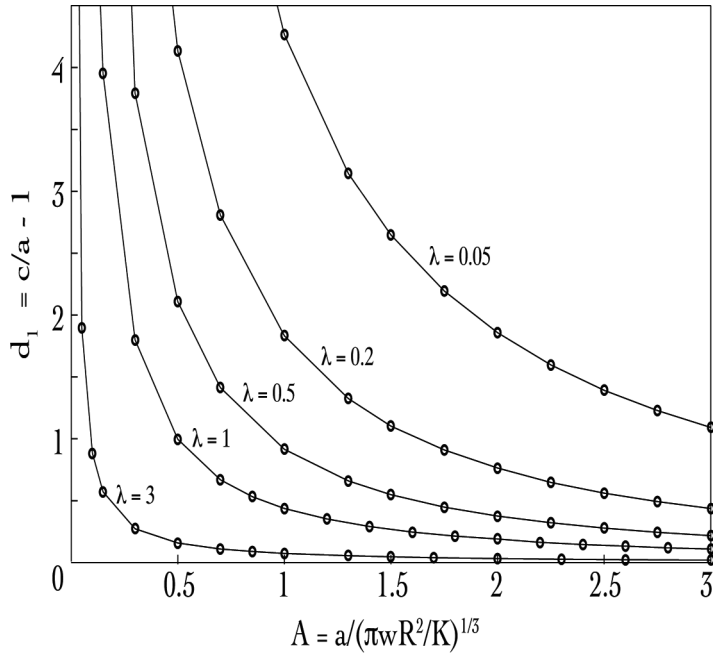


**FIGURE 17** Variation of the scaled adhesive zone,  $c_1$ , with the contact region's non-dimensionalized size,  $A$ , as a function of the adhesive strength,  $\lambda$ .

Figures 14–16 contrasts the  $A - \bar{P}$ ,  $A - \Delta$ , and  $\Delta - \bar{P}$  relationships at several different adhesive strengths for three different layer thicknesses. In Fig. 14, we also show by a dashed gray line at each of the three  $H$  the results obtained in the previous section by extending the JKR approximation to layers. Again, this extended JKR approximation matches well at large  $\lambda$ .

Finally, Fig. 17 displays the variation of the adhesive zone's length,  $d_1 = (c - a)/a$  with the contact region's size,  $A$ , for several values of the adhesive strength,  $\lambda$ . The layer's thickness is kept fixed at  $H = 0.1$ ; it is seen that for a fixed  $\lambda$ ,  $d_1$  hardly changes if  $H$  is varied. We observe that the adhesive zone sharply increases in length *relative* to the contact region when  $A \rightarrow 0$ . This is simply an indication of the fact that the adhesive interaction exists even when the punch touches the layer's surface at only a point, *i.e.*,  $A = 0$ . Also, for a fixed  $A$ ,  $d_1$  increases with decreasing  $\lambda$ . This is easily understood by recalling that  $\lambda$  is the ratio of the adhesive stress,  $\sigma_0$ , to the layer's stiffness,  $K$ , see [14]. Thus, when  $\lambda$  is small, the layer is too stiff to deform and contact the punch due to the tensile stress,  $\sigma_0$ , alone, thereby resulting in a non-contact interaction over a greater area, *i.e.*, a bigger adhesive zone,  $d_1$ . In contrast, for larger  $\lambda$ , the adhesive strength is strong enough to deform the relatively more compliant layer over almost the entirety of the adhesive zone and bring it in contact with the punch's profile,

leading to a much smaller  $d_1$ . In the limit of  $\lambda \rightarrow \infty$ ,  $d_1 \rightarrow 0$ , which is the JKR approximation.

## 5. CONCLUSIONS

In this work, we have extended to the case of two-dimensional indentation of a rigid cylindrical punch into an adhesive elastic layer the adhesive zone model pioneered by [13] for axisymmetric contact of an adhesive elastic half-space. We followed a semi-analytical approach employing Chebyshev polynomials. The Hertzian theory and the JKR approximation were obtained as natural corollaries of our computations. An extremely good match with available exact analyses was demonstrated. The current approach is extremely simple to implement and may also be immediately extended to axi-symmetric contact and/or flexible substrates. The current method works well for thin layers with  $H = b/a \geq 0.07$ . For even thinner layers, in the case of non-adhesive contact, it has been possible to employ the Wiener-Hopf technique to obtain answers; see [4]. We are currently working on adapting that approach to an adhesive zone model for indentation of adhesive thin layers.

## REFERENCES

- [1] Aleksandrov, V. M., *J. Appl. Math. Mech.* **27**, 1410–1424 (1962).
- [2] Aleksandrov, V. M., *J. Appl. Math. Mech.* **28**, 714–717 (1964).
- [3] Aleksandrov, V. M., *J. Appl. Math. Mech.* **32**, 691–703 (1968).
- [4] Meijers, P., *Appl. Sci. Res.* **18**, 353–383 (1968).
- [5] Gladwell, G. M. L., *Contact Problems in the Classical Theory of Elasticity*, (Kluwer, New York, USA, 1980).
- [6] Yu, H. Y., Sanday, S. C., and Rath, B. B., *J. Mech. Phys. Solids* **38**, 745–764 (1990).
- [7] Perriot, A. and Barthel, E., *J. Mater. Res.* **19**, 600–608 (2004).
- [8] Johnson, K. L., Kendall, K., and Roberts, A. D., *Proc. R. Soc. A* **324**, 301–313 (1971).
- [9] Johnson, K. L. and Sridhar, I., *J. Phys. D: Appl. Phys.* **34**, 683–689 (2001).
- [10] Yang, F., *J. Phys. D: Appl. Phys.* **35**, 2614–2620 (2002).
- [11] Yang, F., *J. Phys. D: Appl. Phys.* **36**, 50–55 (2003).
- [12] Barthel, E. and Perriot, A., *J. Phys. D: Appl. Phys.* **40**, 1059–1067 (2007).
- [13] Maugis, D., *J. Colloid Interface Sci.* **150**, 243–269 (1992).
- [14] Sergici, A. O., Adams, G. G., and Müftü, S., *J. Mech. Phys. Solids* **54**, 1843–1861 (2006).
- [15] Johnson, K. L., *Contact Mechanics*, 3rd ed, (Cambridge University Press, Cambridge, UK, 1985).
- [16] Deryaguin, B. V., Muller, V. M., and Toporov, Y. P., *J. Colloid Interface Sci.* **53**, 314–326 (1975).

- [17] Kanninen, M. F. and Popelar, C. H., *Advanced Fracture Mechanics*, (Oxford University Press, New York, USA, 1985).
- [18] Greenwood, J. A. and Johnson, K. L., *J. Phys. D: Appl. Phys.* **31**, 3279–3290 (1998).
- [19] Sneddon, I. N., *Fourier Transforms*, (Dover, New York, 1980).
- [20] Boyd, J. P., *Chebyshev and Fourier Spectral Methods*, 2nd ed., (Dover, New York, USA, 2001).
- [21] Mason, J. C. and Handscomb, D. C., *Chebyshev Polynomials*, (Chapman & Hall/CRC, Boca Raton, Florida, USA, 2003).
- [22] Hamming, R. W., *Numerical Methods for Scientists and Engineers*, 2nd ed., (Dover, New York, USA, 1986).
- [23] Gradshteyn, I. S. and Ryzhik, I. M., *Tables of Integrals, Series and Products*, 6th ed., (Academic Press, London, UK, 2000).
- [24] Popov, G. I., *J. Appl. Math. Mech.* **33**, 503–517 (1969).
- [25] Hills, D. A., Nowell, D., and Sackfield, A., *Mechanics of Elastic Contacts*, (Butterworth-Heinemann, Oxford, UK, 1993).
- [26] Baney, J. M. and Hui, C. Y., *J. Adhesion Sci. Technol.* **11**, 393–406 (1997).